FLOW AND HEAT TRANSFER DYNAMICS IN FUEL CELL COOLING SYSTEMS: A SCALE-RESOLVING COMPUTATIONAL STUDY

Louis Krüger, Suad Jakirlić
Institute of Fluid Mechanics and Aerodynamics, Technical University of Darmstadt
Peter-Grünberg-Strasse 10, 64287 Darmstadt, Germany
krueger.l@sla.tu-darmstadt.de, jakirlic@sla.tu-darmstadt.de

ABSTRACT

This study presents a computational investigation of the fluid dynamics and heat transfer in a fuel cell cooling system, with particular emphasis on its bipolar plate. The specific focus is on a near-wall RANS eddy-viscosity model based on elliptic-relaxation, sensitized to accurately capture turbulent fluctuations by introducing an appropriately modeled production term in the scale-supplying equation, motivated by the Scale-Adaptive Simulation approach (SAS, Menter & Egorov (2010)), proposed by Krumbein *et al.* (2020). This sensitized turbulence model overcomes the need for exceptionally fine mesh resolution, a requirement often associated with conventional Large-Eddy Simulations (LES). The results are compared with those of a reference LES, performed complementarily, in which the Wall-Adapting Local Eddy-viscosity subgrid scale model was used. The simulations are performed using the open source code OpenFOAM® and the pre-processing software ANSA for the meshing of the considered flow configuration. This study provides insight into the flow and thermal fields of a fuel cell cooling system and demonstrates the performance of the proposed turbulence model.

Introduction

The European Union has made a commitment to reduce its greenhouse gas emissions by 40% by 2030 and to achieve greenhouse gas neutrality by 2050. The urgency to reduce greenhouse gas emissions has increased interest in hydrogen as a clean energy source, with fuel cells showing great promise for various applications. Ensuring the safe operation of fuel cells requires a thorough understanding of their cooling systems, particularly the flow and heat transfer within the bipolar plates. The flow within this cooling structure is characterized by complex flow phenomena such as spatially and temporally varying vortical structures, impinging jet and subsequent bifurcation including laminarization within the filigree channels and the exiting jet-like streams experiencing breakup and subsequent transition to turbulence in the outlet pipe. The widely used and computationally affordable Reynolds-Averaged Navier-Stokes (RANS) models are often incapable to properly capture the highly unsteady flow dynamics. In contrast, the scale-resolving LES models are capable to resolve a large part of the turbulent energy spectrum and thus are more reliable in terms of prediction quality and accuracy. However, LES requires a much higher computational effort due to the very fine spatial and temporal resolution required. To overcome the above-mentioned problems, an appropriately sensitized RANS model is used in an LES-relevant, time-accurate computational procedure, thus enabling the capture of the spectral dynamics of turbulence, to an extent consistent with the underlying grid resolution and relevant turbulence quantities, representing the solutions of the corresponding transport equations to be simultaneously solved.

Computational Method

This study employs a robust computational approach to investigate the flow and heat transfer phenomena within the fuel cell cooling system. The basic governing equations of incompressible flow, including continuity and momentum equations, are solved, along with key turbulent quantities such as turbulent kinetic energy (k) and specific dissipation rate (ω). Spatial and temporal derivatives are discretized using second-order accurate schemes to ensure numerical accuracy. Furthermore, computational efficiency is enhanced by employing adaptive time-stepping, where the CFL criterion is set to less than 0.7. This adaptive time-stepping strategy optimizes the computational resources while maintaining accuracy. The eddy-resolving $k-\omega-\zeta-f$ model, denoted as $\mathrm{ER}-\zeta-f$ model, was proposed by Krumbein *et al.* (2020) and represents an efficient scale-resolving unsteady RANS model. It is based on a sensitization of the conventional RANS $k-\omega-\zeta-f$ model by introducing a specifically modeled production term into the ω equation. This four-equation RANS model is based on the $k-\varepsilon-\zeta-f$ formulation of Hanjalić *et al.* (2004), representing a numerically robust upgrade of the $\overline{v'^2}-f$ model of Durbin (1991), who originally introduced an elliptic relaxation methodology in the context of near-wall eddy viscosity models. The quantity ζ is thereby defined as $\zeta=\overline{v'^2}/k$. In contrast to the widely used isotropic turbulence velocity scale $\sqrt{k}$, the intensity of the wall-normal Reynolds stress component $\sqrt{\overline{v'^2}}$ is applied, which is described as a scalar variable behaving similarly to the normal Reynolds stress component when approaching the solid wall. Thus, an effect of near-wall turbulence anisotropy is included in the eddy-viscosity formulation. Finally, Krumbein *et al.* (2020) (see Krumbein (2019) for more details) transformed the ε equation into the equation governing the specific dissipation rate, which represents the inverse time scale ω $(=\varepsilon/k)$. Accordingly, the $k-\omega-\zeta-f$ model was proposed. The formulation of the additional source term P_{SAS} is relevant to the scale-adaptive simulation (SAS) concept of Menter & Egorov (2010). The initially proposed SAS-formulation involving the von Karman length scale ($L_{vK}=\kappa S/|\nabla^2 U|$), was presently reformulated by expressing it as a function of the second derivative of the velocity field directly, as proposed originally by Rotta (1972). The latter modification made the model even more sensitive against turbulence unsteadiness (a resolving mode can be enabled at even coarser grid resolutions). The additional production term P_{SAS} in the ω equation is defined as follows:

$$P_{\mathrm{SAS}} = C_{\mathrm{SAS}} \max\left(\sqrt{\frac{\partial^2 \overline{U}_i}{\partial x_j \partial x_j}\frac{\partial^2 \overline{U}_i}{\partial x_k \partial x_k}}\sqrt{k} - C_{T_2} T_2, 0\right) \quad (1)$$

Interested readers are referred to the original reference for detailed model specification. In order to obtain reference data, an additional simulation was carried out using the Wall-Adapting Local Eddy-viscosity (WALE) subgrid-scale model by Nicoud & Ducros (1999) in a Large-Eddy Simulation.

Computational Details

The cooling channels of a reference bipolar plate, including the inlet and outlet pipes with a diameter of $D = 6$ mm and a length of 90 mm, positioned at a distance of 95.25 mm from each other, are investigated presently. The reference bipolar plate is connected to the inlet and outlet pipes and includes two symmetrical semicircular zones (denoted as conditioning zone & confluence zone) that serve to divide and merge the flow both before and after it passes through the cooling channels. Within the cooling structure, 30 channels with a square cross-section of $\mathrm{H} \times \mathrm{W} = 1 \times 1$ mm, a length of $\mathrm{L} = 43.25$ mm, and rib spacing of 1 mm are present. The coolant used is water mixed with MEG at 50 vol%. The ANSA pre-processing software is used to mesh the computational domain, resulting in three different fully structured meshes. Two grids, containing 14 and 30 million hexahedral volume cells, are employed for applying the $\mathrm{ER} - \zeta - f$ model. An additional mesh of 285 million volume cells is used within the LES. Inlet conditions are set in accordance with the experimental setup, including volume flow rates of 0.2 $^{\mathrm{l}}/_{\mathrm{min}}$ and 1.4 $^{\mathrm{l}}/_{\mathrm{min}}$, representing fully laminar and turbulent flow regimes ($Re_{\mathrm{b}} \approx 5000$, $U_{\mathrm{b}} = 0.825\,^{\mathrm{m}}/_{\mathrm{s}}$), respectively. The inlet temperature is set to 80° C and the total heating rate applied throughout the cooling channels is set to 100 W using a passive scalar transport approach. To provide a detailed analysis of the characteristic areas, the results are evaluated on various slices and characteristic length measures are introduced for simplicity. The correlation between these positions/measures and the geometry is shown in Figures 3 and 10.

Results

Fig. 1 illustrates the flow rate distribution over the cooling channels, providing an understanding of the overall flow topology and the influence of the flow rate. There is a significant difference between the two operating conditions, with a noticeable shift in the flow distribution towards the outermost channels due to the increased flow rate. The flow distribution shown below results from multiple interacting complex flow patterns such as an impingement and distribution area and also influences the flow conditions within the cooling channels and the subsequent confluence region. In the present study, only the flow rate of 1.4 $^{\mathrm{l}}/_{\mathrm{min}}$ will be considered in detail. Given the significance of the inlet region (fully developed pipe flow), particularly for the impingement area, the reference LES data generated can be validated using DNS (Direct Numerical Simulation) data. Fig. 2 shows the velocity, Turbulent Kinetic Energy (TKE) and components of the Reynolds stress tensor (specifically $\overline{u_z u_z}^+$ and $\overline{u_z u_r}^+$) in wall units plotted against the

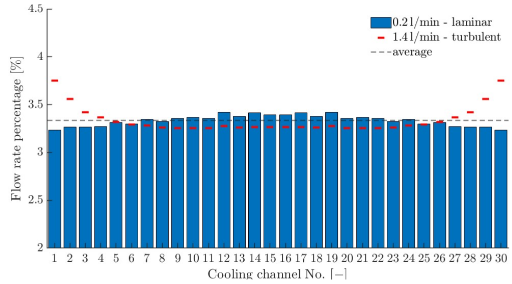

Figure 1: Flow rate distribution over cooling channels.

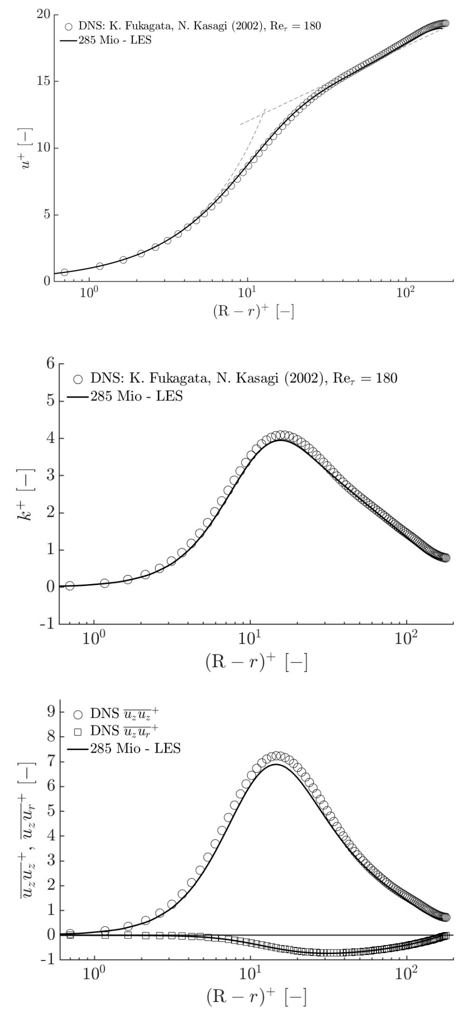

Figure 2: Velocity u^+, TKE k^+ and Reynolds stress component profiles at inlet pipe in wall units.

wall distance. Overall, a good agreement between the LES and DNS data is observed in the inlet region.

The flow enters the domain through a pipe and impinges with a diameter to height ratio of 6:1 on the left side of the bipolar plate. The impingement causes a deflection of the flow and thus a strong streamline curvature. In addition to the ratio $^{k_{\mathrm{SGS}}}/_{k_{\mathrm{total}}}$ ($< 20\%$ in the entire domain), the more strict quality criterion $^{\Delta_{\max}}/_{\eta_{\mathrm{k}}}$ is used to validate the LES. $\Delta_{\max}$ is defined as the maximum grid length of a cell in one direction and η_{k} represents the Kolmogorov length scale. As Pope (2000) pointed out, the ratio should be below 10-12 for a suitable LES, which is fulfilled in the entire domain and is shown as an example for

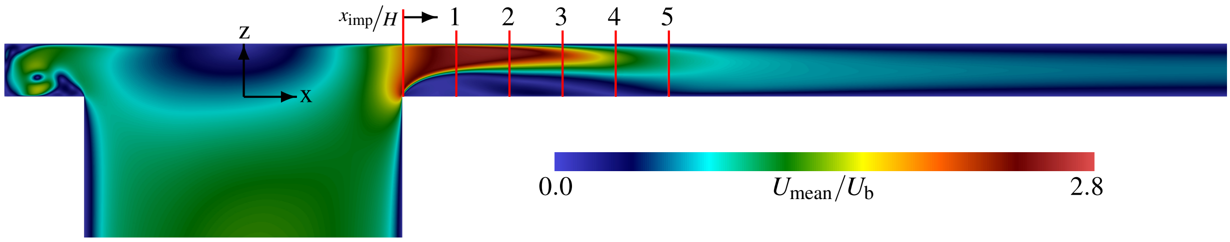

Figure 3: Normalized mean velocity field at the impingement region of the bipolar plate (height $H = 1$ mm) in the symmetry plane ($y = 0$ mm) with marked positions at a distance between $0H$ (left) and $5H$ (right) to the impinging jet center.

the impingement area in Fig. 4 (top).

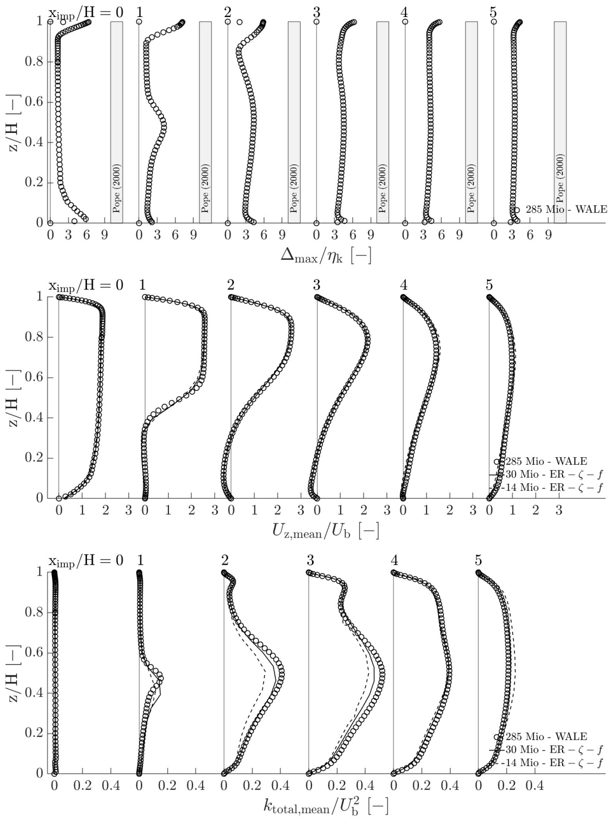

Figure 4: Δ_{max}/η_k, normalized streamwise velocity and TKE distribution at impingement for $x_{imp}/H = 0$ to 5.

As can be seen in the velocity field shown above, the flow is strongly deflected by the impingement and accelerated locally in the upper half of the channel ($z/H = 1$). The flow is not able to follow the sharp edge, resulting in a separation area including recirculation at the lower wall ($z/H = 0$). Due to the high velocity gradient, the shear layer ensures the production of TKE, which appears as a peak in the center of the channel. The ER $-\zeta-f$ model is able to reproduce the complex configuration even on a coarse grid. The deviation of the TKE in the center of the channel for the coarsest grid can be reduced by mesh refinement as shown above. After the impingement a semicircular propagation of the coolant occurs within the flow conditioning zone, aiming to achieve a highly uniform distribution of the cooling fluid into the filigree cooling channels (see Fig. 1). The evolution of the velocity and TKE profile with increasing distance to the impingement ($x_{imp}/H = 5$ to 17) across the distribution area (slice in y-direction) at the channel center ($z/H = 0.5$) is presented in Fig. 6. However, the increased flow rate of 1.4 l/min results in a significant shift of the coolant distribution towards the outer edge of the geometry, causing increasing velocity at the outer area of the distribution zone, which persists until the coolant enters the cooling channels at $x_{imp}/H = 23$. As shown in Fig. 10 the impingement leads to the formation of small turbulent vortex structures providing a peak of TKE in the symmetry line of the bipolar plate ($y = 0$ mm) shown in Fig. 5. The subsequent widening of the computational domain (expanding the range of y) causes a deceleration of the flow in the center area, whereby the local Reynolds number reduces and TKE significantly decreases compared to the impingement area. Although the flow characteristics in this region are strongly linked to the correct capture of the impingement process, there is a very good quantitative agreement between the high-resolution LES and the ER $-\zeta-f$ model simulation with a significantly coarser grid. Even the TKE production as a result of the formation and deflection of the small turbulent structures and the TKE dissipation as a result of the previously discussed processes can be quantitatively accurately captured.

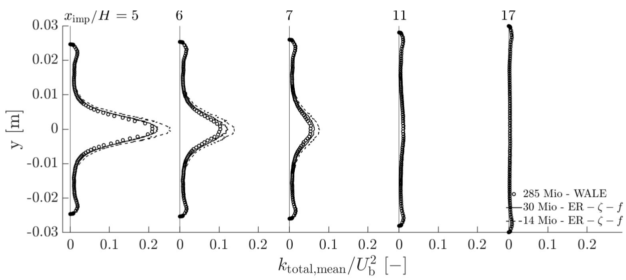

Figure 5: TKE profile development across distribution area at $x_{imp}/H = 5, 6, 7, 11$ and 17.

The flow through the heated cooling channels defines the next characteristic region. Due to the low local Reynolds number within these channels, the flow exhibits a significant change in its characteristics, which results in the subsequent smoothing out of the turbulent fluctuations. Fig. 7 shows the velocity profile after different levels of progression in the cooling channels for two exemplary channels. Channel no. 15 represents an inner channel, while channel no. 2 is typical for an

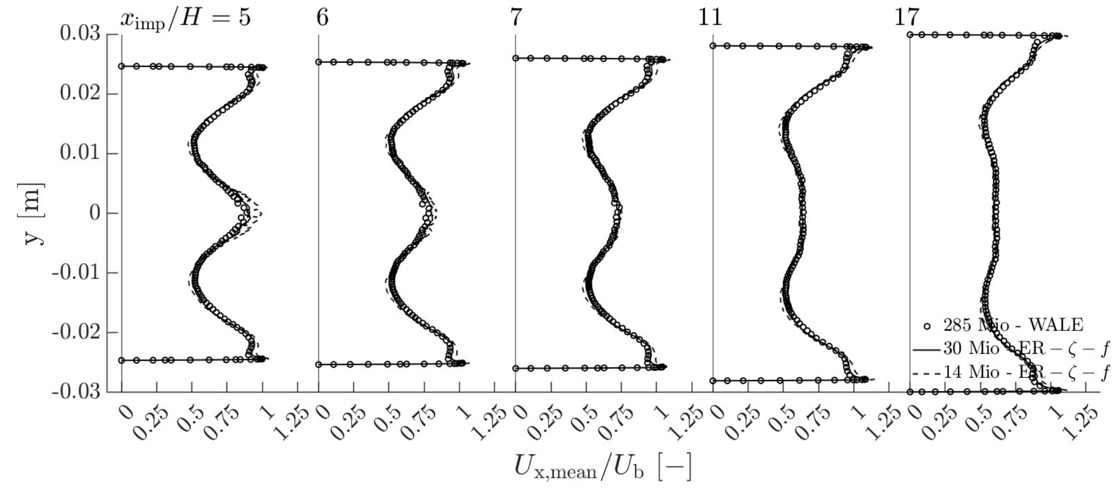

Figure 6: Velocity profile development across distribution area at $x_{\mathrm{imp}}/H = 5, 6, 7, 11$ and 17.

outer channel.

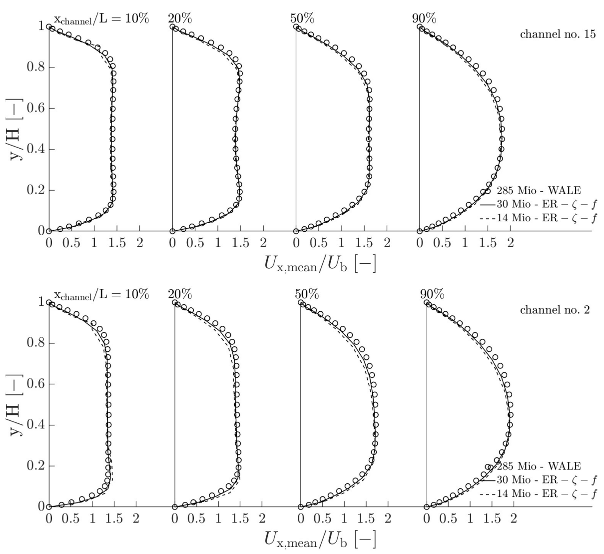

Figure 7: Velocity profile evolution across cooling channels no. 2 and no. 15 at different levels of progression.

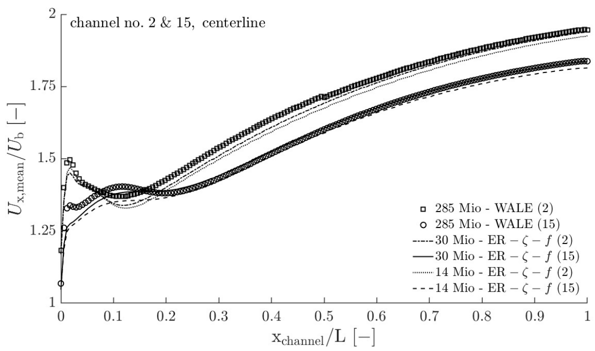

Figure 8: Velocity at the centerline ($y/H = 0.5$) along the cooling channels no. 2 and no. 15.

After a 10% progression, both velocity profiles show a typical turbulent, appropriately flattened shape in the flow core. With further progress, the profiles evolve into a characteristic laminar shape. This transformation occurs in both the inner and outer cooling channels. In general, velocity fields in both channels are similar. During the transformation process, the velocity at the center of the channels ($y/H = 0.5$) increases, as shown in Fig. 8. The figure illustrates the centerline channel velocity from the beginning of the cooling channels ($x_{\mathrm{channel}}/L = 0$) to the end of the cooling channels ($x_{\mathrm{channel}}/L = 1$).

The difference in velocity magnitude between the two paths is caused by the non-homogeneous distribution of flow across the cooling channels. As a result, the outer channel no. 2 experiences a higher velocity in the channel center. Furthermore, the increase in velocity, caused by the transformation of the profile shape, from a turbulent to a laminar-like one, has not been completed until the end of the cooling channel. Therefore, the laminar velocity asymptote has not been fully reached, indicating that the flow regime is not fully developed.

The region downstream of the cooling structures is characterized by the interaction between the jet-like streams, their breakup and the significant deflection of the primary flow as it enters the outlet pipe (cf. Fig. 10). The merging of the volume flows from the individual cooling channels, together with the steep gradients created by the deflection, re-establishes a fully turbulent pipe flow within the outlet pipe. The confluence region shows entirely different phenomena compared to the geometrically identical distribution region. Immediately after the cooling channels, the mutual interaction of the jet-like streams is still rather low, which are separated from each other by detachment regions including recirculation as shown in Fig. 9 (top).

Starting at about $x_{\mathrm{confluence}}/H = 5$, a stronger interaction between the flow regions takes place, leading to the breakup of the jet-like streams and to complex mixing. These extremely reactive processes are sensitive to the grid resolution, hence a somewhat larger deviation between the LES and the results of the coarser simulations can be seen here. In general, the

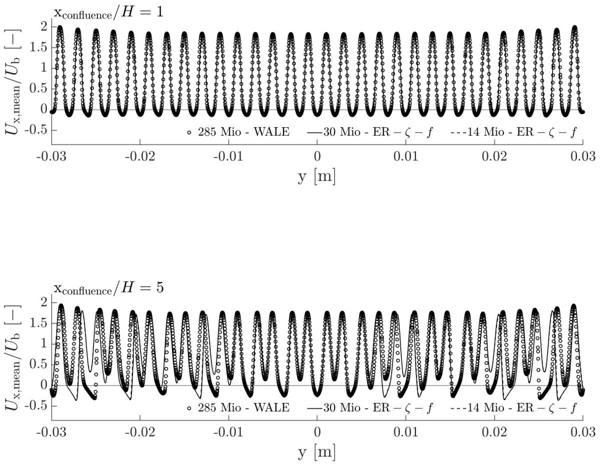

Figure 9: Velocity distribution across confluence area in $y-$direction at locations $x_{\mathrm{confluence}}/H = 1$ and 5, cf. Fig. 10

topology of the streams and the recirculation areas can be reproduced well, although not to the extent shown in the velocity magnitude evolution in Fig. 9 (bottom).

Since the present study is concerned with the cooling system of a fuel cell and the channel structure is supplied with a total heat flow of 100 W, the heat transfer dynamics within the system are analyzed in more detail. As can be seen from Fig. 11 (left), the recirculation areas behind the ribs heat up strongly up to $\Delta\Theta \sim 6$ K. Convection then causes the hot and less heated areas to mix. The interaction of the jet-like streams and their breakup also ensure a high degree of mixing. As mentioned above, the confluence region is followed by a deflection into the pipe, where a fully turbulent flow is re-established. This strong deflection of the flow again ensures enhanced mixing, which can be seen locally in high $u'\theta'$ values, causing that the outlet pipe has an almost homogeneous temperature field established after a short distance. Finally, $\Delta\Theta$ at the outlet is equivalent to its theoretical value of 1.175 K (at 100 W heating rate).

Conclusion

This study examines the complex flow and heat transfer dynamics within a fuel cell cooling system, focusing on a reference bipolar plate. The configuration shows a sequence of complex flow phenomena. To ensure the reliability of the results, the reference LES data is validated in the inlet region using DNS data and within the complex domain due to several quality criteria. First the fully developed turbulent pipe flow as a basis for subsequent interactions is observed. The subsequent impinging jet introduces significant flow deflection, initiating the formation of small turbulent vortex structures that cause a peak in TKE. The flow distribution is shifted to the outer edge of the geometry and undergoes a significant expansion before the coolant enters the cooling channels. This results in higher flow rates in the outermost cooling channels. Inside the filigree cooling channels, the flow exhibits a significant change in its characteristics, ending up in the characteristic shape of a laminar velocity profile, but not fully developed. As the channels are heated by a constant heat flux rate, the temperature inside the channels increases in the vicinity of the wall, which is relevant for the subsequent confluence region. The jet-like streams are separated by recirculation areas and strongly interact with each other within the confluence region, leading to break-up. This, together with the converging geometry, results in enhanced mixing. Downstream, a sharp 90^o deflection into the outlet pipe re-establishes a fully turbulent pipe flow and produces a homogeneous temperature field after a short distance driven by enhanced mixing processes.

The study includes a comparative analysis between the well-resolved LES (using WALE) and the Eddy-Resolving $\zeta - f$ model on coarser meshes, resulting in a significantly reduced computational time. For instance, while the LES occupies 1.5 million CPU hours to reach a converged solution, the $\mathrm{ER} - \zeta - f$ model with 14 million computational cells requires about 100.000 CPU hours. Likewise, the model with 30 million grid cells utilizes around 220.000 CPU hours. In general, the $\mathrm{ER} - \zeta - f$ model is able to obtain comparable results in all complex flow regions, including not only the velocity field but also the TKE production and dissipation. It is a suitable and robust model for complex and highly coupled systems, as demonstrated in fuel cell cooling systems.

In summary, this study provides insights into the complex interactions of flow and heat transfer phenomena within fuel cell cooling systems. These findings enhance the overall understanding of such systems and provide avenues for optimizing designs and predicting weaknesses, thereby improving overall system performance and efficiency.

REFERENCES

Durbin, Paul A. 1991 Near-wall turbulence closure modeling without "damping functions". *Theoretical and Computational Fluid Dynamics* **3**, 1–13.

Hanjalić, K., Popovac, M. & Hadžiabdić, M. 2004 A robust near-wall elliptic-relaxation eddy-viscosity turbulence model for CFD. *International Journal of Heat and Fluid Flow* **25** (6), 1047–1051.

Krumbein, B. 2019 A modeling framework for scale-resolving computations of turbulent flow over porous and rough walls. Phd thesis, Technical University of Darmstadt.

Krumbein, B., Maduta, R., Jakirlic, S. & Tropea, C. 2020 A scale-resolving elliptic-relaxation-based eddy-viscosity model: development and validation. *New Results in Numerical and Exp. Fluid Mech. XII, (NNFM)* **142**, 90–100.

Menter, F. & Egorov, Y. 2010 The scale-adaptive simulation method for unsteady turbulent flow predictions. part 1: Theory and model description. *Flow, Turbulence and Combustion* **85**, 113–138.

Nicoud, F. & Ducros, F. 1999 Subgrid-scale stress modelling based on the square of the velocity gradient tensor. *Flow Turbulence and Combustion* **62**, 183–200.

Pope, S. B. 2000 *Turbulent Flows*. Cambridge University Press.

Rotta, Julius C. 1972 *Turbulente Strömungen*. Stuttgart: Teubner Verlag Stuttgart.

Acknowledgments. Based on a decision taken by the German Bundestag, the project was supported by the Federal Ministry for Economic Affairs and Climate Action (BMWK) and the AIF (German Federation of Industrial Research Associations eV) within the framework of the industrial collective research (IGF) program (IGF- No.: 22097 N/1). The authors furthermore acknowledge the computing time granted on the Lichtenberg HPC of the Technical University of Darmstadt. The authors wishes to thank the Customer Service of BETA CAE Systems.

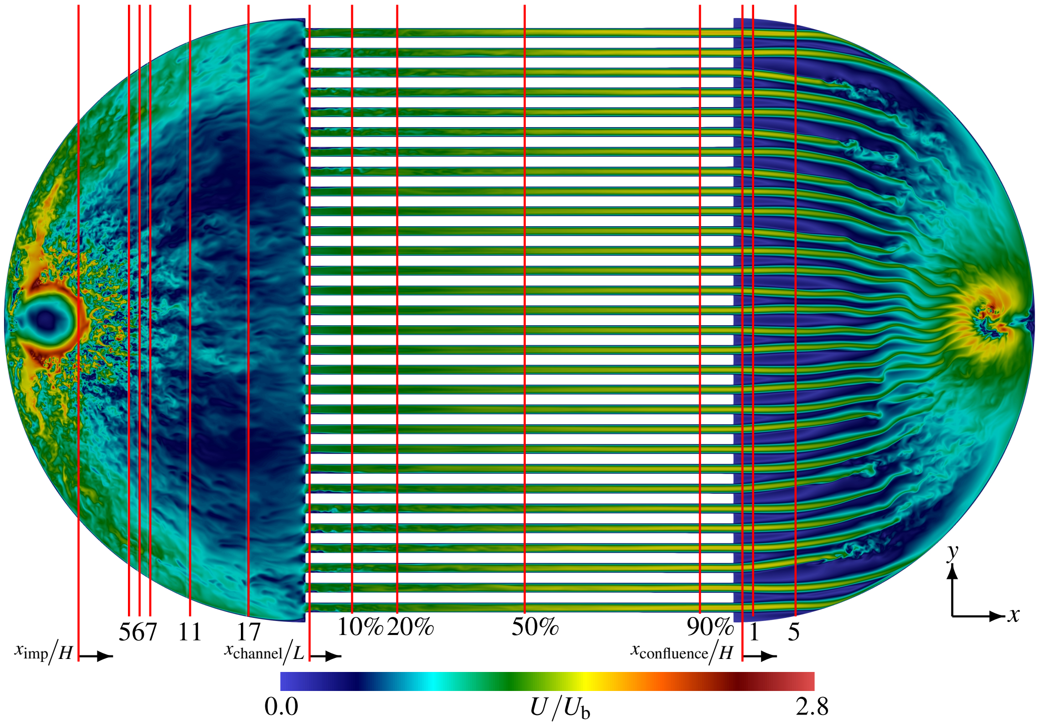

Figure 10: Instantaneous velocity field at the center of the bipolar plate ($z/H = 0.5$) obtained by the LES (285 mio. volume cells) with marked positions and characteristic length measures for the impingement and distribution region (x_{imp}/H), the cooling channels ($x_{channel}/L$) and the confluence area ($x_{confluence}/H$).

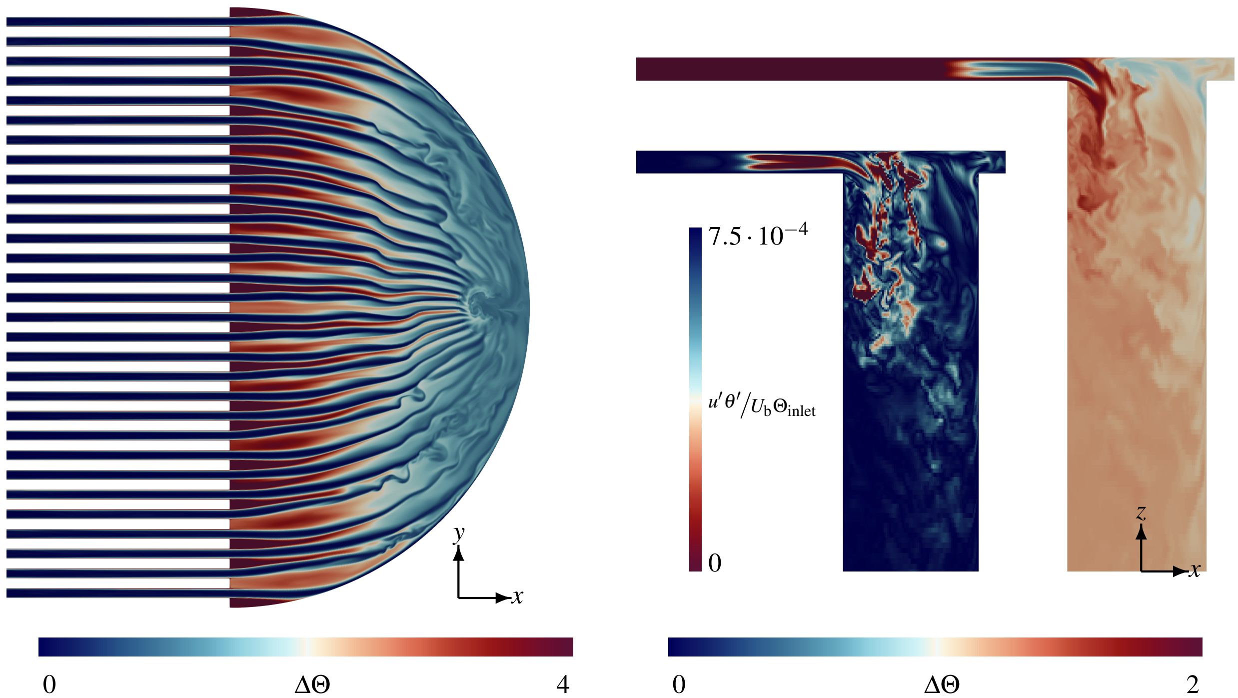

Figure 11: Instantaneous temperature field $\Delta\Theta = \Theta - \Theta_{inlet}$ at the center of the bipolar plate ($z/H = 0.5$) within the confluence area (left), at the outlet pipe at the symmetry plane ($y = 0$ mm) (right) and turbulent heat flux $u'\theta'$ obtained by the ER $- \zeta - f$ model (30 mio. volume cells).